

# **Quantifying the demographic vulnerabilities of dry woodlands to climate and competition using range-wide monitoring data**

3

4

5

6

## **Running Head: Range-wide demographic vulnerabilities**

7

8

Robert K. Shriver<sup>1,2\*</sup>, Charles B. Yackulic<sup>3</sup>, David M. Bell<sup>3</sup>, John B. Bradford<sup>3</sup>

9

10

<sup>1</sup>Ecology Center, Utah State University

11

<sup>2</sup>Department of Natural Resources and Environmental Sciences, University of Nevada-Reno

12

13

14

15

16

17

18  
10

21

22

24

28    **Abstract**

29    Climate change is expected to alter the distribution and abundance of tree species, impacting  
30    ecosystem structure and function. Yet, anticipating where this will occur is often hampered by a  
31    lack of understanding of how demographic rates, most notably recruitment, vary in response to  
32    climate and competition across a species range. Using large-scale monitoring data on two dry  
33    woodland tree species (*Pinus edulis* and *Juniperus osteosperma*), we develop an approach to  
34    infer recruitment, survival, and growth of both species across their range. In doing so, we  
35    account for ecological and statistical dependencies inherent in large-scale monitoring data. We  
36    find that warming and drying conditions generally lead to declines in recruitment and survival,  
37    but there were some idiosyncrasy in the strength of responses across species. Climate conditions  
38    lead to vulnerable regions, such as *Pinus edulis* in N. Arizona, where both survival and  
39    recruitment are low. Our approach provides a path forward for leveraging emerging large-scale  
40    monitoring and remotely sensed data to anticipate the impacts of global change on species  
41    distributions.

42    Keywords: climate, competition, demography, *Pinus edulis*, *Juniperus osteosperma*

43    **Introduction**

44    Changing climate, disturbance regimes, and human activity are expected to reshape the  
45    distribution of forest and woodland species across the globe, potentially transforming the  
46    structure of these ecosystems (Allen et al. 2010, McDowell et al. 2018). Although, mortality of  
47    overstory plants are often the most obvious indicators of declining forest and woodland health  
48    (e.g. Millar and Stephenson 2015), the resilience and long-term viability of tree species in the  
49    face of environmental change will be determined by not only the survival of existing individuals,  
50    but also the recruitment and growth of new individuals that drive population recovery and

51 spread, i.e. resilience (Jackson et al. 2009). Evidence of declining forest health and resilience due  
52 to declining recruitment is increasingly common (Petrie et al. 2017, Stevens-Rumann et al.  
53 2018). Yet anticipating where forest and woodland species may be most vulnerable to  
54 environmental change is often hampered by a lack of understanding of how rates of survival,  
55 growth, and, most notably, recruitment vary across a species range and the environmental  
56 conditions driving them.

57 Demographic processes are increasingly recognized to be critical to understanding  
58 species range shifts and ecosystem state changes in response to climate change (Briscoe et al.  
59 2019). But, efforts to estimate how plant recruitment, survival, and growth vary across large  
60 spatial scales are limited, in part because many traditional demographic inference approaches  
61 (e.g. Easterling et al. 2000) do not typically accommodate diverse data structures and the  
62 ecological/statistical dependences inherent to large spatial data. Instead, plant demographic  
63 analyses have typically placed the onus on researchers to mark and return to individuals and  
64 independently measure each demographic transition in the field, making it logistically  
65 challenging to scale data collection to larger areas. At the same time, there has been an explosion  
66 of diverse datasets from large-scale field monitoring and remote sensing (e.g. Forest Inventory  
67 and Analysis Database, lidar) with the potential to revolutionize our understanding of spatio-  
68 temporal plant demographic processes and their population consequences. Yet, these data  
69 sources rarely provide data on both survival and recruitment at the individual-scale resolution  
70 required for traditional demographic modeling approaches. Harnessing the power of these  
71 datasets will require flexible modeling approaches that can link detailed, individual demographic  
72 data with additional data sources that describe how demographic processes drive changes in

73 abundance and population structure across large landscapes and over decades (Shriver et al.  
74 2019).

75 Here, we develop an approach to infer the range-wide recruitment, survival, and growth  
76 rates of two widespread dry woodland species using large-scale Forest Inventory and Analysis  
77 (FIA) data. Because FIA plots encompass nearly the entire range of many tree species, they  
78 present a unique opportunity to understand how demographic rates vary across a species' range  
79 and identify where populations may be most vulnerable to changing climate and disturbance.  
80 But, FIA data also present a number of challenges (see Methods for full explanation), most  
81 notably accounting for ecological dependencies in quantifying recruitment. Specifically,  
82 seedlings are not tagged but simply counted, thus the fate (growth/survival) of existing seedlings  
83 are not independently quantified from new recruits. We overcome this challenge by developing  
84 an integrated population modeling approach that accounts for ecological dependencies while also  
85 accounting for spatial autocorrelation and sharing information across sites in a rigorous way.

86 **Methods**

87 *FIA Data*

88 We developed our demographic models using the publicly available FIA database  
89 (<http://www.fia.fs.fed.us/>). FIA is a systematic and standardized survey of forested regions in the  
90 entire United States, including both public and private lands. Full details on the sampling design  
91 can be found in Bechtold and Patterson (2005).

92 We focus our analyses on two widespread dry woodland species in the Colorado Plateau  
93 and Great Basin regions: *Pinus edulis* (hereafter PiEd) and *Juniperus osteosperma* (hereafter  
94 JuOs). Nearly the entire ranges of both species are within the United States, thus FIA data  
95 provide a near complete survey of their range-wide dynamics. Because our primary focus was

96 quantifying demographic rates of each species and linking these to climate across their range, we  
97 excluded all plots in which fire mortality or tree harvesting occurred. This resulted in 2,013 plots  
98 with 16,951 tagged PiEd individuals, and 2,380 JuOs plots with 25,105 tagged JuOs individuals.  
99 All PiEd and JuOs individuals greater than 15.24 cm (6 in.) in height are surveyed. Within each  
100 plot, all adult trees greater than 12.7 cm (5 in.) diameter are assigned unique tags and tracked  
101 within 4, 7.32 m (24 ft.) radius subplots. All saplings <12.7 cm & > 2.54 cm (1 in.) diameter are  
102 assigned unique tags and tracked within 4, 2.07 m (6.8 ft.) radius microplots within the larger  
103 adult plots. Finally, seedlings <2.54 cm diameter are counted within the same microplots as the  
104 saplings.

105 Two censuses were conducted 10 years apart in each plot. In some cases, additional plot  
106 surveys occurred between the standard 10 year interval. These additional surveys were excluded  
107 because they were sporadic and not standardized across the dataset. The exact timing of the  
108 initial censuses varied by state and region within state (typically 10-20% of plots in each state are  
109 surveyed each year) but occurred between 2000 and 2007.

110 *Demographic Modeling*

111 Data on adult and sapling growth and survival are collected at the individual level.  
112 Individual plants >2.54 cm diameter are tagged, and as a result the growth and survival of an  
113 individual plant can be tracked over the census interval. We develop growth (i.e. change in size)  
114 and survival models following the well-developed generalized linear model functional forms  
115 common for plant demography models (Rees et al. 2014). Individual diameter size change is  
116 modeled as

117 
$$z_{i,t+1} \sim Normal(u_{i,t}, \sigma^2) \quad [1]$$

118 
$$u_{i,t} = \alpha_{(z)} z_{i,t} + \mathbf{X}_{d[i]} \mathbf{b}_{(z)} + \omega_{d[i]} \quad [2]$$

119 Where  $z_{i,t}$  is the size of plant  $i$  ( $i=1 \dots I$ ) in the first census ( $t$ ),  $\alpha_{(z)}$  is a regression coefficient for  
120 plant size,  $\mathbf{X}_{d[i]}$  is a vector of plot-level environmental covariates for plot  $d$  ( $d=1 \dots D$ ) where  
121 individual  $i$  is located,  $\mathbf{b}_{(z)}$  is a vector of environmental regression parameters specific to the size  
122 model,  $\omega_{d[i]}$  is a plot-level spatial random effect, and  $\sigma$  is a variance parameter.

123 Similarly, survival probability is modeled as

124  $s_{i,t+1} \sim Bern(p_{i,t})$  [3]

125  $logit(p_{i,t}) = \alpha_{(s)} z_{i,t} + \mathbf{X}_{d[i]} \mathbf{b}_{(s)} + \delta_{d[i]}$  [4]

126 where  $p_{i,t}$  is the probability of survival for individual  $i$  from  $t$  to  $t+1$ ,  $z_{t,i}$  is again the size of plant  
127  $i$  in the first census ( $t$ ),  $\alpha_{(s)}$  is a regression coefficient for plant size on survival,  $\mathbf{b}_{(s)}$  is a vector  
128 of environmental regression parameters specific survival, and  $\delta_{d[i]}$  is a plot-specific spatial  
129 random effect for each individual  $i$ . Note, the comparatively small number of observed JuOs  
130 mortality events led spatial random effects to be non-identifiable, thus were not included in the  
131 JuOs survival model.

132 Spatial random effects were fit using a predictive process model (Banerjee et al. 2008,  
133 Latimer et al. 2009). Predictive process models address the computational challenges of fitting  
134 spatial models to large datasets by reducing point locations (i.e. plots) to a lesser number of  
135 constituent knots that encapsulate the landscape of spatially autocorrelated processes not  
136 explained by covariates. In the case of growth random effects,

137  $\boldsymbol{\omega}^* \sim MVN(0, \Sigma^*)$  [5]

138  $\Sigma_{k,k'}^* = \tau_{(z)} e^{-\phi_{(z)} \delta_{k,k'}}$  [6]

139  $\boldsymbol{\omega} = \Sigma_{(\omega, \omega^*)} \Sigma^{*-1} \boldsymbol{\omega}^*$  [7]

140      $\omega^*$  is a K-length vector of random effects ( $\omega^* = \omega_1^*, \omega_2^*, \dots, \omega_K^*$ ) associated with each knot ( $k$ ).  
141      $\Sigma^*$  is a covariance matrix where each element is a correlation among knots weighted by  
142     distance,  $\delta_{k,k'}$ .  $\phi$  is a parameter describing the rate at which correlations decay as a function of  
143     distance (km), and  $\tau$  is an error term.  $\omega$  is a D-length vector of random effects for each plot  
144     ( $\omega_d = \omega_1, \omega_2, \dots, \omega_D$ ). The underlying knot-based spatial landscape is then linked back to specific  
145     plots using Eq. 7, where  $\Sigma_{(\omega, \omega^*)}$  is a cross-covariance matrix which describes the spatial  
146     relationship between plots ( $\omega$ ) and knots ( $\omega^*$ ) using Eq. 6, where in this case  $\delta_{k,k'}$  is the distance  
147     (km) between each the fuzzed location of plot ( $d$ ) and knot ( $k$ ) pair. While model fit will improve  
148     as the number of knots increase, the choice of the number of knots is a tradeoff of model fit and  
149     computational efficiency. We follow the recommendations of Latimer et al. 2009 (i.e. 100-400  
150     knots) by using 200 knots who's locations are assigned to maximize coverage of FIA plot  
151     locations using the “cover.design” function in the “fields” package (v. 9.6) in R (Nychka and  
152     Furrer 2017).

153           FIA data present several challenges for estimating recruitment rates. First, unlike the  
154     growth and survival of saplings and adults, the recruitment, growth, & survival of seedling is  
155     never directly observed. All conifers <2.54 cm diameter but >15.25cm height are simply  
156     counted, making it impossible to directly separate new recruits from the fate of pre-existing  
157     seedlings. In other words, the change in the count from census to census represents both new  
158     recruitment, but also the survival and growth of existing plants. While this data structure does  
159     not preclude inference on the underlying reproduction rate, it is incompatible with most  
160     traditional statistical approaches (e.g. Poisson GLMs) for estimating plant reproduction  
161     recruitment, which require clearly identifying the reproductive output (e.g. seeds) of existing  
162     individuals and the fate of these propagules.

163           Second, the search area for seedlings is small given the low density of seedlings, and  
164   considerably smaller than area adult trees are measured over (~12x smaller). This presents a  
165   challenge for estimating recruitment because as the number of individuals in a plot declines  
166   separating the true signal of environmental and spatial processes from noise introduced by  
167   sampling and demographic stochasticity is increasingly difficult. This may be particularly  
168   problematic for tree species exhibiting spatially and temporally heterogeneous seedling  
169   distributions, such as woodland tree species (Bell et al. 2014).

170           To address these challenges, we developed an integrated size-structured population  
171   modeling approach that shares available information among our different datasets (i.e.  
172   growth/survival of adults/saplings and counts of seedlings) and across FIA plots to infer the  
173   growth and survival of seedlings along with the reproductive output of existing trees leading to  
174   new recruits. Because the fate of all tagged individuals in the first census (i.e. any individual  
175   >2.54 cm) is already known, our goal is to build a model that describes the fate of all untagged  
176   individuals. Untagged individuals include all plants <2.54 cm and any plants that were not  
177   tagged in the first census, but reached the minimum tagged size (2.54 cm) by the second census.  
178   Plants reaching the 2.54 cm threshold in the second census could comprise existing plants  
179   previously <2.54 cm or new recruits.

180           We model the number of untagged plants in a plot as conditionally Negative Binomial

$$\mathbf{c}'_{d,t+1} \sim Neg. Binomial(\mathbf{n}'_{d,t+1} * a, \kappa) \quad [8]$$

181           Where  $\mathbf{c}'_{d,t+1}$  is a 5x1 vector of the counts of all untagged plants in plot  $d$  at the second census  
182    $t+1$ .  $\mathbf{n}'_{d,t+1}$  is a 5x1 vector of area standardized occurrence rates.  $a$  is the total plot area in which  
183   plants were counted. And,  $\kappa$  is a dispersion parameter. Each element in  $\mathbf{c}'_{d,t+1}$  represents the  
184   counts of individuals in each 2.54 cm (or 1 inch) diameter class up to 12.7 cm. While the choice  
185   counts of individuals in each 2.54 cm (or 1 inch) diameter class up to 12.7 cm. While the choice

186 of diameter class is flexible, we use the natural choice of 2.54 cm diameter classes for all trees  
187 because the FIA dataset already lumps any plants <2.54 cm into a single class. Only plants less  
188 than 12.7 cm (i.e. size classes 1 to 5) were considered because untagged plants larger than this  
189 are more likely a results of previous missed observations than growth and recruitment from the  
190 smallest classes.  $\mathbf{n}'_{d,t+1}$  is defined as

191 
$$\mathbf{n}'_{d,t+1} = \mathbf{A}_{d,t} \mathbf{n}_{d,t} \quad [9]$$

192 Where  $\mathbf{A}_{d,t}$  is a 5 x 30 ( $h=1\dots5, j=1\dots30$ ) discretized integral projection model (IPM) kernel (i.e.  
193 a matrix projection model with 2.54 cm size classes) describing all the pathways by which an  
194 existing plant could lead to an untagged plant (survival/growth of existing plants <2.54 cm and  
195 new reproduction from existing plants).  $\mathbf{n}_{d,t}$  is a 30x1 vector of area standardized rates of  
196 occurrence of all plants in the first census in each 2.54 cm bin, derived from the empirical counts  
197 of all plants.

198  $\mathbf{A}_{d,t}$  is made up by the two different pathways by which untagged plants may appear: 1)  
199 the growth/survival of plants that were <2.54 cm in the previous census, and 2) recruitment  
200 arising from reproduction of existing trees.

201 
$$A_{h,j} = \overbrace{g_{h,1} * s_1}^{10.1} + \overbrace{r_h * f_j}^{10.2} \quad [10]$$

202 The first term (10.1) describes the fate of individuals <2.54 cm at time  $t$ .  $g_{h,1}$  are growth  
203 transition probabilities describing the movement of individuals in size class 1 to size classes 1 to  
204 5.  $s_1$  is the survival probability of individuals in size class  $j=1$  at time  $t$ . The second term (10.2)  
205 describes the number of new recruits produced per existing plant in each size class,  $f_j$ , and the  
206 probability new recruits will transition to size class  $h$  by the second census. Note each element in  
207 Eq. 10 would also be indexed by site ( $d$ ) and census interval ( $t$ ), but we have omitted this for  
208 clarity.

209 Like tagged plants,  $g_{h,1}$  is defined by a normal distribution, but here it is a discretized  
210 kernel to account for size class binning. For a given site,  $d$ ,

211 
$$g_{h,1} = (\Phi(Upper_h|u_d, \sigma^2) - \Phi(Lower_h|u_d, \sigma^2))/\Phi(0|u_d, \sigma^2) \quad [11]$$

212 Where  $\Phi$  indicates a cumulative normal distribution with mean  $u$  and variance  $\sigma^2$  evaluated at  
213 the upper and lower size limit of size bin  $h$  (Doak et al, In Revision). The final term renormalizes  
214 the kernel to strictly positive size values to prevent biologically impossible transitions to  
215 negative sizes.  $u$  is the same function used to evaluate the growth of tagged individuals (see eqs.  
216 1 and 2), but in this case individual size ( $z_{i,t}$ ) is approximated by the midpoint of bin  $j=1$ ,  $m_1$

217 
$$u_d = \alpha_{(z)}m_1 + \mathbf{X}_d \mathbf{b}_{(z)} + \omega_d \quad [12]$$

218  $s_1$  is also based on the same survival function used for tagged plants, again approximated by the  
219 midpoint of bin  $j=1$  ( $m_j$ ).

220 
$$s_1 = logit(p_d) = \alpha_{(s)}m_1 + \mathbf{X}_d \mathbf{b}_{(s)} + \delta_d \quad [13]$$

221  $r_h$  uses a Gaussian kernel (normalized to sum to 1) to estimate the probability of any new recruit  
222 reaching size classes 1 to 5 as

223 
$$r_h = N(m_h|\nu, \nu^2) / \sum_{i=1}^5 N(m_h|\nu, \nu^2) \quad [14]$$

224 Finally, the function of primary interest is the number of new recruits produced per  
225 existing tree of size  $j$ ,  $f_j$ .

226 
$$\log(f_{j,d}) = \alpha_{(f)}m_j + \mathbf{X}_d \mathbf{b}_{(f)} + \gamma_d \quad [15]$$

227 Where  $f_{j,d}$  is the number of new recruits produced per adult of size  $j$  at across all 30 size classes.  
228  $m_j$  is the midpoint of each of the size classes, and  $\alpha_{(f)}$  is a regression parameter describing the  
229 effect of size on reproduction.  $\mathbf{b}_{(f)}$  are regression parameters describing the impact of size on

230 reproductive output, and  $\gamma_d$  is a spatial random effect again defined by a predictive process (see  
231 Eq. 5) with its own parameters  $\phi_{(f)}$  and  $\tau_{(f)}$ .

232 *Covariates*

233 Based on previous research in dry woodland ecosystems, covariates in  $\mathbf{X}_d$  were selected to  
234 summarize the effects of moisture availability (MA), heat stress (HS), and neighbor density (ND)  
235 on the growth, survival, and recruitment (McDowell et al. 2008, Allen et al. 2010). Moisture  
236 availability was the mean growing season (May to October) available soil water (i.e.  $>-3.9$  MPA)  
237 over 40 to 100 cm depth over the 10-year census interval. Heat stress was the average  
238 temperature over the growing season over the 10-year census interval. Neighbor density was the  
239 basal area density of all living trees in the plot at the first census.

$$\mathbf{X}_d = [1, \text{MA}_d, \text{MA}_d^2, \text{HS}_d, \text{HS}_d^2, \text{ND}_d ]$$

240 Squared MA and HS terms were added to account for possibility of nonlinear responses of  
241 species to environmental conditions across their range. Although multi-model inference using  
242 differing variables and functional form is possible given unlimited time (models take about 5-8  
243 days to fit), we chose instead to focus on a limited set of variables and functional forms that are  
244 common to the demographic modeling literature and well supported based on our prior  
245 knowledge of the biology of Piñon and Juniper. All covariate parameters were given non-  
246 informative priors. Further details and covariates, model fitting, and priors can be found in the  
247 Supplemental Material.

248 **Results**

249 To understand how vital rates vary across climate and geographic space we estimated  
250 posterior mean demographic rates for a 15 cm diameter individual using the observed moisture  
251 availability, heat stress, and neighbor density in each plot as well as plot random effects. This

252 allowed us to quantify and visualize how vital rates change with each climate variable, while still  
253 taking into account the considerable spatial variability that can be introduced from other climate  
254 conditions (e.g. a dry-warm vs. dry-cool plot) and unaccounted for environmental conditions (i.e.  
255 random effects).

256 *Climate and competition*

257 Model results indicate consistent responses in both JuOs and PiEd recruitment to climate.  
258 In both species, recruitment increased, on average, as moisture availability increased, saturating  
259 or declining slightly in the wettest conditions (Figs. 1 & 2). JuOs and PiEd recruitment decreased  
260 with both increasing neighbor density and heat stress, but the overall magnitude of recruitment  
261 change due to heat stress is smaller than moisture availability and neighbor density. Both species  
262 showed consistent increases in recruitment output with plant size (Table S3 & S4).

263 Posterior mean probabilities of survival were far more variable across plots for PiEd (0.2-  
264 1) than JuOs (0.98-1) (Figs. 1 & 2). In fact, the number of observations of JuOs mortality not  
265 associated with fire or harvest was only 153 individuals (0.6% of 25,015), compared to 1,597  
266 (9.4% of 16,951) for PiEd. In contrast to recruitment, increasing heat stress led to clear declines  
267 in survival. JuOs and PiEd individuals in the coolest plot are expected to have 10-year survival  
268 probabilities near 1. PiEd survival rates were declined by ~10-15% in the driest conditions, while  
269 JuOs survival declined ~1%. Plots with higher neighbor density and lower moisture availability  
270 are also estimated to have lower PiEd survival (Fig. 3), but JuOs showed no consistent survival  
271 changes across the gradient in neighbor density or moisture availability. There was little effect  
272 of individual size on survival, and estimates overlap with 0 (Table S3 & S4).

273 Growth (i.e. change in diameter size) increased on average for PiEd with increasing  
274 moisture availability and declining temperatures (Fig. 1). In contrast, JuOs showed little

275 consistent growth response to moisture availability and increasing growth with warmer  
276 temperatures (Fig. 2). Both species showed clear and consistent declines in diameter growth with  
277 increasing neighbor density and plant size, but the decrease in diameter growth with size is in  
278 part due to the radial growth geometry, and may not represent declines in overall biomass growth  
279 at larger sizes. (Table S1).

280 *Geographic Space*

281 We found limited evidence of consistent responses of either species' demographic rates  
282 to single geographic gradients (latitude, longitude, elevation), except increasing survival at high  
283 latitudes/elevations and declining growth at high elevations in JuOs (Fig. 3, S11, & S12).  
284 However, we did find clear hotspots including low survival and recruitment in PiEd in the 4  
285 corners, lower survival and higher recruitment for JuOs in southwest Utah. We also found  
286 regions of high survival for both JuOs and PiEd in their northwestern range, with survival  
287 generally declining towards their central and southern range (Fig. 3, S11, & S12).

288 **Discussion**

289 Our approach offers a promising step forward in leveraging non-traditional  
290 spatiotemporal datasets to understand the link between plant demographic rates and large scale  
291 abundance and distribution patterns (Briscoe et al. 2019). An explosion of large-scale monitoring  
292 and remote sensing dataset provide exciting opportunities to understand the drivers of species  
293 abundance and distributions, but these datasets are rarely fully compatible with traditional  
294 demographic modeling approaches (e.g. Easterling et al. 2000). For example, in our study, FIA  
295 data provide detailed information on individual growth and survival, yet recruitment of new  
296 individuals was not directly observed. To overcome this, we developed integrated modeling  
297 approach that simultaneously inferred the fate of existing seedling as well as new seedlings

298 entering the population through recruitment. Using FIA data and novel demographic inference  
299 approaches, we found that variation in abiotic climate conditions (heat stress and moisture  
300 availability) and biotic conditions (neighbor density) can both help explain variation in the  
301 recruitment, survival, and growth of woodland species across their range. Similar modeling  
302 approaches that link individual- and population-scale data provide exciting opportunities to  
303 improve our understanding and predictions of how individual demographic rates translate into  
304 population changes over time and across landscapes (Shriver et al. 2019).

305 PiEd exhibited a much greater variability in survival rates, and greater sensitivity of  
306 growth and survival to heat stress and moisture availability than JuOs. This finding compliments  
307 a growing body of work which have found regional mortality in pinyon pine associated with  
308 drought and heat waves, and link the greater mortality rates in pinyon compared to juniper  
309 species to differences physiological responses to warming and drying and susceptibility of PiEd  
310 to pine beetle during drought (McDowell et al. 2008, Allen et al. 2010). Considerably less is  
311 known about environmental conditions that drive PiEd and JuOs recruitment. Consistent with  
312 findings from other semi-arid tree species (Petrie et al. 2017, Stevens-Rumann et al. 2018), we  
313 found that increasing moisture is generally associated with increasing recruitment in both JuOs  
314 and PiEd. But we also found evidence that recruitment rates may level-off, or begin to decline, in  
315 the wettest conditions. Evidence that increasing temperatures will lead directly to declining  
316 recruitment were more equivocal. With modest declines in PiEd recruitment, but no clear  
317 response in JuOs.

318 Together our results indicate that future warming and drying conditions, as are expected  
319 throughout the SW (Garfin et al. 2013), will likely lead to declines in survival and recruitment  
320 and increasing demographic vulnerabilities of PiEd and JuOs. Quantitatively assessing the

321 likelihood and speed of forest decline at different locations will require integrating these  
322 demographic vulnerabilities into population models, and will be the focus of future work. We  
323 also find potential opportunities for management to alleviate the impacts of climate change.  
324 Increases in tree density lead to notable declines in all vital rates (except JuOs survival).  
325 Managed reductions in tree density could provide an opportunity to increase individual growth  
326 and decrease the risk of widespread mortality (Bradford and Bell 2017). Similarly, increases in  
327 recruitment associated with declining density could provide a natural compensatory mechanism  
328 enabling resilience of some populations following mortality events.

329 **Acknowledgments**

330 This work was supported by the USGS North Central Climate Adaptation Science Center. We  
331 thank Caitlin Andrews for her assistance in preparing climate covariates. Any use of trade, firm,  
332 or product name is for descriptive purposes only and does not imply endorsement by the U.S.  
333 Government.

334 **References**

- 335 Allen, C. D., A. K. Macalady, H. Chenchouni, D. Bachelet, N. McDowell, M. Vennetier, T.  
336 Kitzberger, A. Rigling, D. D. Breshears, E. H. (Ted) Hogg, P. Gonzalez, R. Fensham, Z.  
337 Zhang, J. Castro, N. Demidova, J. H. Lim, G. Allard, S. W. Running, A. Semerci, and N.  
338 Cobb. 2010. A global overview of drought and heat-induced tree mortality reveals emerging  
339 climate change risks for forests. *Forest Ecology and Management* 259:660–684.  
340 Banerjee, S., A. E. Gelfand, A. O. Finley, and H. Sang. 2008. Gaussian predictive process  
341 models for large spatial. *J R Stat Soc Series B Stat Methodol.* 70:825–848.  
342 Bechtold, W. a., and P. L. Patterson. 2005. The enhanced forest inventory and analysis program -  
343 national sampling design and estimation procedures:85.

- 344 Bell, D. M., J. B. Bradford, and W. K. Lauenroth. 2014. Early indicators of change: Divergent  
345 climate envelopes between tree life stages imply range shifts in the western United States.  
346 *Global Ecology and Biogeography* 23:168–180.
- 347 Bradford, J. B., and D. M. Bell. 2017. A window of opportunity for climate-change adaptation:  
348 easing tree mortality by reducing forest basal area. *Frontiers in Ecology and the*  
349 *Environment* 15:11–17.
- 350 Briscoe, N. J., J. Elith, R. Salguero-Gómez, J. J. Lahoz-Monfort, J. S. Camac, K. M. Giljohann,  
351 M. H. Holden, B. A. Hradsky, M. R. Kearney, S. M. McMahon, B. L. Phillips, T. J. Regan,  
352 J. R. Rhodes, P. A. Vesk, B. A. Wintle, J. D. L. Yen, and G. Guillera-Arroita. 2019.  
353 Forecasting species range dynamics with process-explicit models: matching methods to  
354 applications. *Ecology Letters* 22:1940–1956.
- 355 Easterling, M. R., S. P. Ellner, P. M. Dixon, and N. Mar. 2000. Size-Specific Sensitivity :  
356 Applying a New Structured Population Model. *Ecology* 81:694–708.
- 357 Garfin, G., A. Jardine, R. Merideth, M. Black, and S. LeRoy. 2013. Assessment of Climate  
358 Change in the Southwest United States. National Climate Assessment.
- 359 Jackson, S. T., J. L. Betancourt, R. K. Booth, and S. T. Gray. 2009. Ecology and the ratchet of  
360 events: Climate variability, niche dimensions, and species distributions. *Proceedings of the*  
361 *National Academy of Sciences of the United States of America* 106:19685–19692.
- 362 Latimer, A. M., S. Banerjee, H. Sang, E. S. Mosher, and J. A. Silander. 2009. Hierarchical  
363 models facilitate spatial analysis of large data sets : a case study on invasive plant species in  
364 the northeastern United States. *Ecology Letters* 12:144–154.

- 365 McDowell, N. G., S. T. Michaletz, K. E. Bennett, K. C. Solander, C. Xu, R. M. Maxwell, and R.  
366 S. Middleton. 2018. Predicting Chronic Climate-Driven Disturbances and Their Mitigation.  
367 Trends in Ecology and Evolution 33:15–27.
- 368 McDowell, N., W. T. Pockman, C. D. Allen, D. D. Breshears, N. Cobb, T. Kolb, J. Plaut, J.  
369 Sperry, A. West, D. G. Williams, and E. a Yepez. 2008. Mechanisms of plant survival and  
370 mortality during drought: why do some plants survive while others succumb to drought?  
371 The New phytologist 178:719–39.
- 372 Millar, C. I., and N. L. Stephenson. 2015. Temperate forest health in an era of emerging  
373 megadisturbance. Science 349:823–826.
- 374 Nychka, D., and R. Furrer. 2017. fields: Tools for spatial data. R Package  
375 Petrie, M. D., J. B. Bradford, R. M. Hubbard, W. K. Lauenroth, C. M. Andrews, and D. R.  
376 Schlaepfer. 2017. Climate change may restrict dryland forest regeneration in the 21st  
377 century. Ecology 98:1548–1559.
- 378 Rees, M., D. Z. Childs, and S. P. Ellner. 2014. Building integral projection models: A user's  
379 guide. Journal of Animal Ecology 83:528–545.
- 380 Shriver, R. K., C. M. Andrews, R. S. Arkle, D. M. Barnard, M. C. Duniway, M. J. Germino, D.  
381 S. Pilliod, D. A. Pyke, J. L. Welty, and J. B. Bradford. 2019. Transient population dynamics  
382 impede restoration and may promote ecosystem transformation after disturbance. Ecology  
383 Letters 22: 1357-1366
- 384 Stevens-Rumann, C. S., K. B. Kemp, P. E. Higuera, B. J. Harvey, M. T. Rother, D. C. Donato, P.  
385 Morgan, and T. T. Veblen. 2018. Evidence for declining forest resilience to wildfires under  
386 climate change. Ecology Letters 21:243–252.
- 387

388 **Figure 1. Response of *Pinus edulis* (PiEd) recruitment, survival, and size to moisture**  
389 **availability, heat stress, and neighbor density.** Posterior mean estimates of a 15 cm diameter  
390 individual for each plot (points) are aggregated into boxplots. Growth is calculated as the change  
391 in size from the size model. Each boxplot spans a width of climate space (x-axis) that includes  
392 10% of the total plots, i.e. each boxplot has an equal number of plots. Boxplot heights along y-  
393 axis span the spatial variability in plots created by additional climate conditions and plot random  
394 effects.

395

396 **Figure 2. Response of *Juniperus osteosperma* (JuOs) recruitment, survival, and growth to**  
397 **moisture availability, heat stress, and neighbor density.** Posterior mean estimates of a 15 cm  
398 diameter individual for each plot (points) are aggregated into boxplots. Growth is calculated as  
399 the change in size from the size model. Each boxplot spans a width of climate space (x-axis) that  
400 includes 10% of the total plots, i.e. each boxplot has an equal number of plots. Boxplot heights  
401 along y-axis span the spatial variability in plots created by additional climate conditions and plot  
402 random effects.

403

404 **Figure 3. Spatial variation in recruitment, survival, and growth for PiEd and JuOs.**

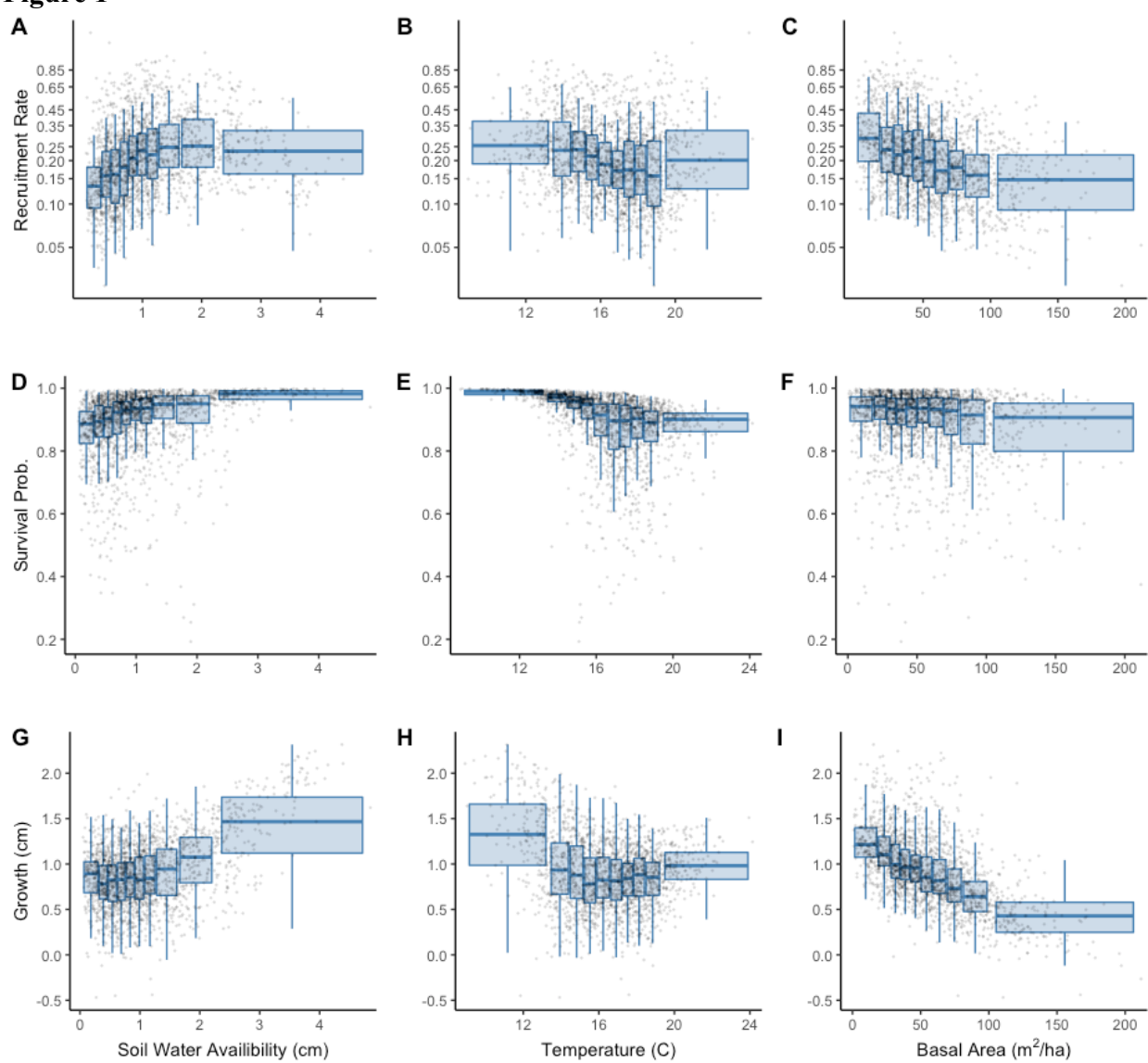
405 Posterior mean estimates of a 15 cm diameter individuals recruitment rate, survival probability,  
406 and growth at all plots (points) in response to climate, competition, and unaccounted for  
407 environmental variation (random effects). Growth is calculated as the change in size from the  
408 size model. Note, points are fuzzed plot locations from publicly available FIA data.

409

410

411

412 **Figure 1**



413  
414

415

416

417

418

419

420

421

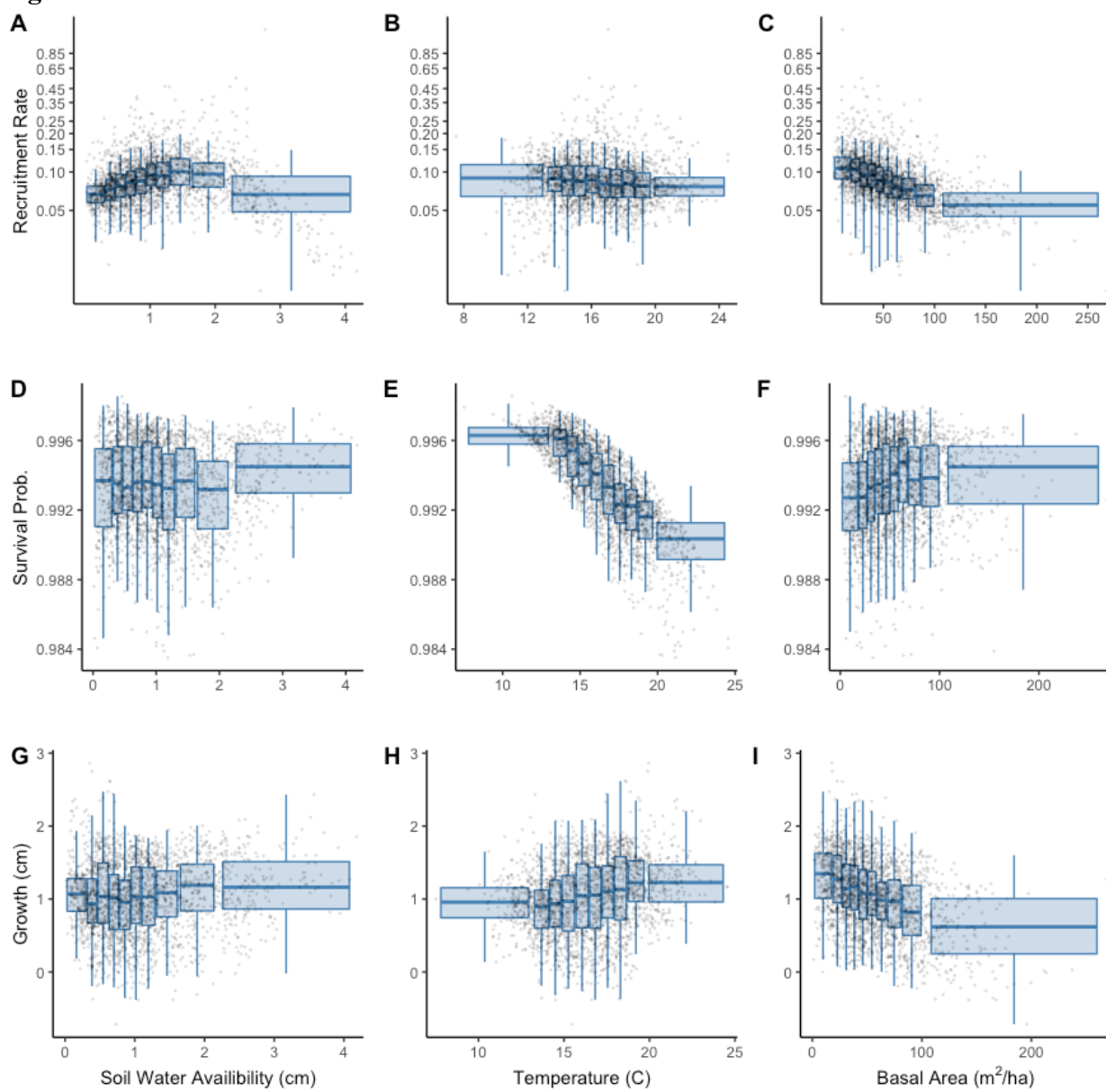
422

423

424

425

426 **Figure 2**



427

428

429

430

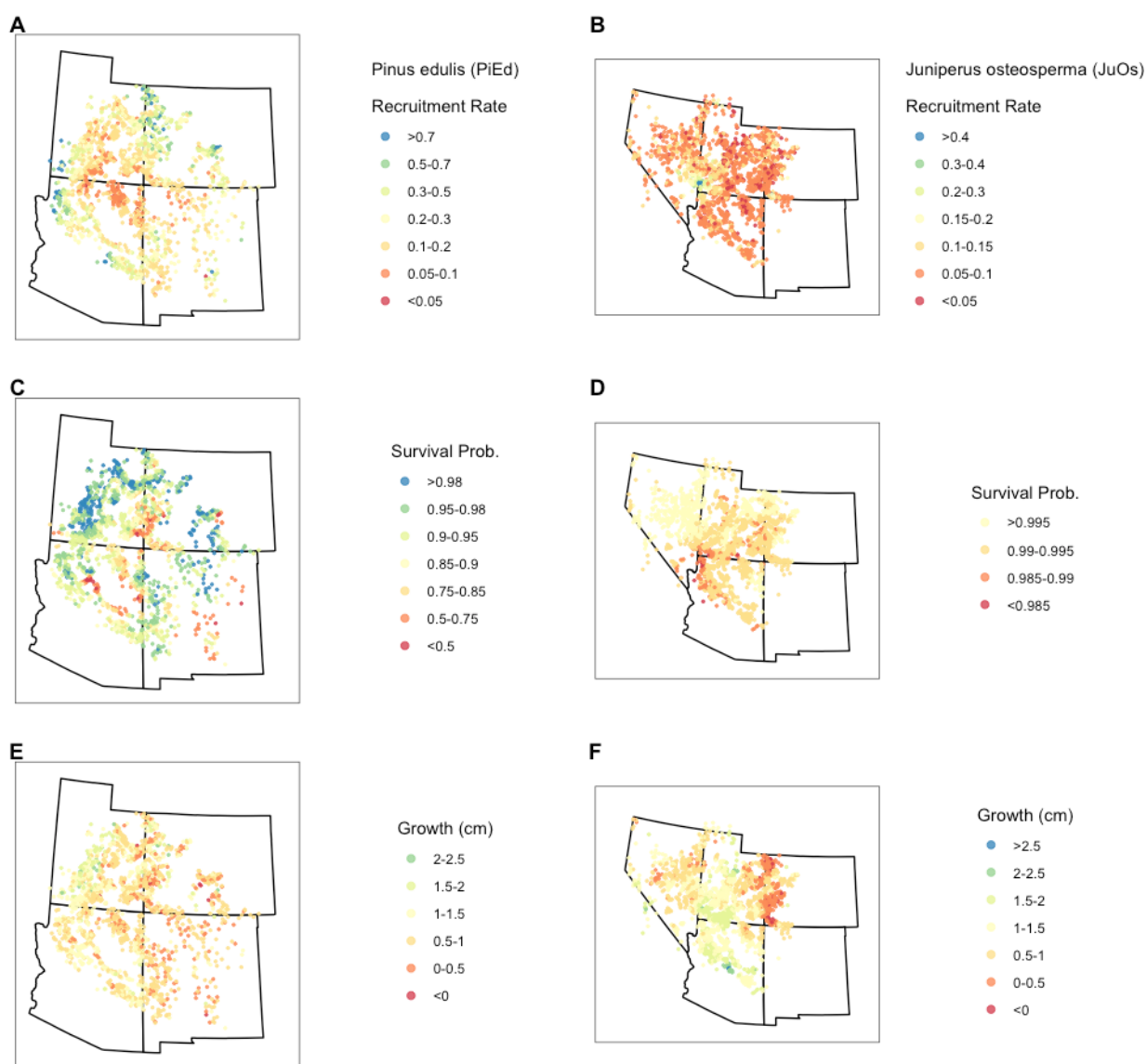
431

432

433

434

435 **Figure 3**



436

437

438